SCIENCE CHINA
Technological Sciences

Metal-support interaction controlled migration and coalescence of supported particles

SuLei HU and Wei-Xue LI

Citation: SCIENCE CHINA Technological Sciences **62**, 762 (2019); doi: 10.1007/s11431-018-9407-3

View online: http://engine.scichina.com/doi/10.1007/s11431-018-9407-3

View Table of Contents: http://engine.scichina.com/publisher/scp/journal/SCTS/62/5

Published by the Science China Press

SCIENCE CHINA
Technological Sciences

SCIENCE CHINA
Technological Sciences

Special Topic: Current Progress in Solid Mechanics and Physical Mechanics
•Article•

May 2019 Vol.62 No.5: 762–772
https://doi.org/10.1007/s11431-018-9407-3

Metal-support interaction controlled migration and coalescence of supported particles

HU SuLei[1,2] & LI Wei-Xue[1,2*]

[1] *Department of Chemical Physics, School of Chemistry and Materials Science, iCHeM, CAS Excellence Center for Nanoscience, University of Science and Technology of China, Hefei 230026, China;*
[2] *Hefei National Laboratory for Physical Sciences at the Microscale, University of Science and Technology of China, Hefei 230026, China*

Received October 13, 2018; accepted December 6, 2018; published online March 29, 2019

The particle migration and coalescence (PMC) kinetics of a supported metal are the main deactivation mechanisms restricting the successful industrialization of nanoparticles, but the theoretical insights regarding these kinetics are lacking. One key issue is the lack of a physical model to predict the effects of metal-support interaction (MSI) on PMC kinetics. In this paper, we report a theoretical study of PMC kinetics and their dependence on MSI. A new particle diffusion model is proposed based on the surface premelting hypothesis that considers the contact angle of a hemispherical particle on the support. Enhanced MSI suppresses PMC by increasing the radius of curvature and the interfacial adhesion energy, even though the accompanying reduction in the geometry factor partially promotes PMC kinetics. The increased surface energy increases the chemical potential of the atoms in the particle, which is conducive to PMC; an increased surface energy also results in enhanced MSI, which suppresses PMC. The competition between these two contradictory effects leads to a critical contact angle where the surface energy has no influence on the diffusion and resulting PMC kinetics. The proposed diffusion theory mode lincluding the effects of the support and the corresponding kinetic simulations, shed light onto the support-dependence of PMC kinetics and provide a foundation for further optimization and design of supported particles with better stability.

particle migration and coalescence, metal-support interaction, supported particles, diffusion coefficient, Smoluchowski

Citation: Hu S L, Li W X. Metal-support interaction controlled migration and coalescence of supported particles. Sci China Tech Sci, 2019, 62: 762–772, https://doi.org/10.1007/s11431-018-9407-3

1 Introduction

The migration and coalescence process for particles across a support surface is of great importance to a variety of fields, including the thermal management of microelectronic devices and many self-assembly and filtration processes, especially nanocatalyst sintering [1–7]. Theoretical work has been performed to try to understand the support-dependence of supported particle sintering kinetics. Two distinct metal-support interactions, namely, the metal particle-support interaction and the metal atom-support interaction, are differentiated. Though the strong metal particle-support interaction stabilizes the supported particles, the strong metal atom-support interaction lowers the total activation energy and dramatically decreases the Ostwald ripening onset temperature and half-life [8]. The support showed significant modulation effects on improving the dispersion [9], electrocatalysis activity [10] and interaction strength [11] of single metal atoms. Density functional theory (DFT) calculations provided direct insights into the strong metal-support interaction (SMSI) [12,13], explaining the increased sintering resistance of nanoparticles supported on a two-composition oxide [12]. Molecular dynamics and reactive force field simulations can model metal-support interactions (MSI) with increasing accuracy and thus yield detailed insights into the dynamic behavior of metal particles supported on dif-

*Corresponding author (email: wxli70@ustc.edu.cn)

ferent substrates [14]. On an ideal flat surface, the diffusion of a nanodroplet remarkably depends on the contact angle according to molecular dynamics simulation [15]. Increasing the MSI is believed to be helpful in suppressing the diffusion of supported particles, improving the sintering resistance [2,16–21]. However, systematic theoretical study of metal-support interaction-dependent particle migration and coalescence (PMC) kinetics has not yet been reported.

The nanoparticle diffusion determines the coalescence rate of the nanoparticles on the support, which is essential for improving the sintering resistance for industrial applications [22–24]. Many particle diffusion mechanisms were investigated under the limitations of very weak or extremely strong interactions. For weak interactions, the supported particles diffuse in various ways, including rotating, rolling, sliding, sticking and so-called "Lévy-flight", where the particle has an almost spherical shape without any apparent contact or wetting on the support surface [25–35]. In the strong case, the supported particles exist in two-dimensional islands. An island migrates by means of the random displacement of its center of mass caused by the fluctuations in its shape. The fluctuations are induced by three processes: the evaporation and condensation of atoms on the border, the migration of atom vacancies across the island, and the diffusion of atoms along the edge [15,36–40]. However, a particle diffusion model able to consistently describe 3D dewetting particles and 2D wetting islands doesn't yet exist. The key issues arise not only from the complexity in describing the collective cooperative motion of a number of atoms but also from the impacts of various factors, including the particle morphology [41], surface composition [41–43], wetting behavior [44,45], substrate surface reconstruction, defects [46–48], reactants [49,50], impurities [51] and support heterogeneity [52–56].

The diffusion theoretical models commonly referenced are based on the work of Gruber [57] regarding the diffusion behavior of a spherical bubble in a bulk material. Willertz et al. [58] realized that the rate of bubble motion may not be limited by the motion of atoms across the bubble surface but by the rate at which atoms leave their positions in the lattice and become mobile on the bubble surface. Thus, it is proposed that the rate of motion of a faceted bubble is determined by the frequency of the nucleation of steps or "pillboxes" on the faceted surface, instead of the time required for atoms to move from a step on one side of the bubble to another step on the other side. The nucleation frequency determines the rate of bubble motion, and a nucleation step is required to form new atomic layers on the surfaces of faceted bubbles.

Using a similar idea, Morgenstern et al. [59] and Khare et al. [60] proposed a theoretical model describing the motion of a two-dimensional vacancy island on Ag(111). Jak et al. [61] introduced the dependence of the nanoparticle surface atom density on the particle size. An extra parameter k was formally introduced to represent the effects of the density and the type of defects on the support surface. It is assumed that k depends on the interaction strength of the defects with the particles without any further specific developments [46]. Behafarid et al. [62] believed that the failure to include the support effects in diffusion models resulted in the discrepancies between the simulated and experimental results.

Mechanistic application of the Gruber diffusion model without any improvements eventually leads to a nanoparticle diffusion rate that is independent of the supports [46,61–63], which is obviously not reasonable. Thus, a diffusion model needs to be developed for a supported particle with a contact angle α on a support that considers the contribution from the metal-support interactions to the diffusion behavior. For a given particle volume, the contact angle α determines the length of the contact perimeter between the particle and the support, which to a certain extent reflects the capability of transferring atoms at one time; on the other hand, the contact angle also affects the tendency of the chemical potential of the atoms in the supported particle to vary with size when the support changes [2]. In this paper, a new particle diffusion model based on the surface premelting [64,65] phenomenon and the Nernst-Einstein relation [66] is presented. The support-dependence of the migration and the resulting coalescence kinetics of supported particles are studied by numerically simulating the Smoluchowski ripening process [67,68].

2 Derivation of the diffusion coefficient

The diffusion coefficient of a supported particle that reasonably includes the support-dependence is the key to simulate the PMC kinetics. The particle is not entirely spherical but is more likely hemispherical due to the sitting on the support and the exposure of part of the particle to vacuum. The influence of the interfacial interaction between the particle and its support should be inherently included.

When the temperature reaches a certain level, the surface atoms of the supported particle premelt and randomly flow (so-called surface premelting [64,65]), so the particle as a whole moves randomly in a Brownian fashion on the support surface [69,70]. As shown in Figure 1, in the premelting state, the subsurface atoms move toward the surface of the particle and easily migrate on the surface and vice versa. With the flow of atoms on the particle surface, any infinitesimal net force breaks the regular tidal fluctuation and leads to a net displacement. The particle as a whole can even randomly diffuse provided that the atoms flow energetically enough on the particle surface, i.e., their diffusion length $(D_s t)^{1/2}$ is comparable to the particle diameter $2r$, where D_s is the diffusion coefficient of the surface atom, r is the radius of

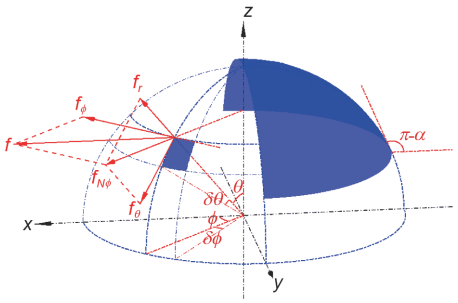

Figure 1 (Color online) A schematic figure representing the diffusion model of a supported nanoparticle. The Cartesian coordinate system is set so that *x*-axis runs along the direction of the fictitious force *f*, which is randomly selected parallel to the support surface, and the *z*-axis is perpendicular to the support surface. α is the contact angle of the particle. The square blue patch is the surface unit area corresponding to the elevation θ and the azimuth ϕ in spherical coordinates. f_ϕ, $f_{N\phi}$, f_r, and f_θ are the projected components along the azimuth direction, the direction normal to the azimuth direction, the radial direction, and the elevation direction, respectively. f_ϕ, $f_{N\phi}$ and the force *f* are in the same plane parallel to the *xy* plane, and $f_{N\phi}$, f_r, and f_θ are in the same plane defined by the *r*-direction and the *z*-axis.

curvature of the particle, and *t* is the characteristic diffusion time. At an elevated temperature, the transient accumulation of the atoms on one side of the particle due to random fluctuations causes its center of mass to move by one atomic distance. These events, randomly repeated many times, drive the Brownian motion of the particle. According to this particle diffusion mechanism, at the atomic level, any motion of an atom contributes to the small lateral displacement of the particle center of mass. The magnitude of this contribution heavily depends on the orientation of the atom on the particle surface [59,60].

The migration velocity of a hemispherical particle due to the random fluctuation of its surface atoms can be calculated by assuming a fictitious driving force *F*. The force can be considered to be a sum of the forces *f* applied to the individual atoms constituting the particle. The Nernst-Einstein relation [66] indicates that if the driving force *F* is exerted on the particle, the instantaneous moving velocity of the particle *V* is proportional to the diffusion coefficient of the particle *D* and can be represented as

$$V = D / kTF. \tag{1}$$

We assume that the particle is a spherical cap with a radius of curvature *r* and a contact angle α (Figure 1). The atoms inside the particle do not contribute to the overall migration of the particle. The atoms in contact with the support do not instantly move relative to the support. Only the surface atoms move along the *x*-axis direction, driven by the force *f*, which is the atomic component of the instantaneous force *F*. The flux j_s due to the flow of atoms across the unit length on the surface is the product of the surface atom density C_p and the moving velocity *V*, which is shown in eq. (1) [66]. This flux is

$$j_s = C_p V = C_p D_s f / kT, \tag{2}$$

where D_s is the atomic diffusion coefficient on the particle surface, *k* is the Boltzmann constant, *T* is the temperature, C_p is the surface atom density, and *f* is the component of force *F* acting on the individual atom. The projection component of the force *f* along the azimuth direction ϕ is $f_\phi = f\sin\phi$. The component along the elevation θ is $f_\theta = f\cos\phi\cos\theta$. The rate at which a surface atom moves along the direction normal to the surface is equal to the rate of the change in volume per unit area. Mathematically, the instantaneous rate $\bar{v}(\phi,\theta)$ of the surface atoms driven by *f* can be represented by the product of the atom volume Ω and the negative divergence of the atomic flux. The unit area is represented by a patch of the surface between a constant azimuth ϕ of width $r\sin\theta\Delta\phi$ and a constant elevation θ of width $r\Delta\theta$. The product of the flux per unit length and the line segment length $r\Delta\theta$ gives the flux entering the patch by crossing the line at the amplitude $\phi+\Delta\phi$

$$j_\phi^+ = C_p D_s f \sin(\phi+\Delta\phi) r\Delta\theta / kT. \tag{3}$$

The flux leaving the patch by crossing the line at ϕ is

$$j_\phi^- = C_p D_s f \sin\phi r\Delta\theta / kT. \tag{4}$$

Similarly, the product of the flux per unit length and the line segment length $r\sin\theta\Delta\phi$ gives the flux entering the patch by crossing the line at the elevation θ

$$j_\theta^+ = C_p D_s f \cos\phi\cos\theta r\sin\theta\Delta\phi / kT. \tag{5}$$

The flux leaving the patch by crossing the line at θ is

$$j_\theta^- = C_p D_s f \cos\phi\cos(\theta+\Delta\theta) r\sin(\theta+\Delta\theta)\Delta\phi / kT. \tag{6}$$

Since the area of the patch is $r^2\sin\theta\Delta\phi\Delta\theta$, the migration rate of the atoms along the direction normal to the surface in the unit surface area, i.e., the divergence of the flux, is

$$\begin{aligned}\bar{v}(\phi,\theta) &= \frac{\mathrm{d}\rho(\phi,\theta)}{\mathrm{d}t} \\ &= \lim_{\Delta\phi\to 0}\Omega\frac{(j_\phi^- - j_\phi^+)+(j_\theta^- - j_\theta^+)}{r^2\sin\theta\Delta\phi\Delta\theta} \\ &= -2C_p D_s \Omega f\cos\phi\sin\theta / kTr,\end{aligned} \tag{7}$$

where $j_\phi = -C_p D_s f\sin\phi / kT$ is the projection component of the atomic flux along the azimuth ϕ.

$j_\theta = C_p D_s f\cos\phi\cos\theta / kT$ is the projection component of the flux along the elevation θ.

The force *f* on a surface atom is related to the equivalent force *F* on the particle by considering the work done by the force *F* in moving the particle a distance *l* [57]. This work (*Fl*) is equivalent to the work done by the force *f* in moving all the atoms in the particle a distance *l* with the atom number $4\pi r^3\alpha_1 / 3\Omega$ in the opposite direction, where the volume factor $\alpha_1 = (2-3\cos\alpha-(\cos\alpha)^3)/4$. It follows that

$$f = 3\Omega F / 4\pi r^3\alpha_1. \tag{8}$$

By substituting eq. (8) into eq. (7), we obtain

$$\bar{v}(\phi,\theta)=\frac{2C_pD_s\Omega}{kTr}\frac{3\Omega}{4\pi r^3\alpha_1}F\cos\phi\sin\theta. \tag{9}$$

Regardless of the contact angle α, the azimuth ϕ and elevation θ in eq. (9) vary from 0 to 2π and 0 to π, respectively. The velocity $\bar{v}$ of the surface atoms normal to the surface is highly dependent on the azimuth ϕ and elevation θ. This velocity first decreases and then increases when θ increases from 0 to π. When $\pi/2<\phi<3\pi/2$, this value is negative, indicating that the surface atoms move inward. Conversely, the positive velocities for $0<\phi<\pi/2$ or $3\pi/2<\phi<2\pi$ mean that the surface atoms move outward. When $\phi=0$ or π, the surface atoms move the furthest inward or outward. When $\phi=\pi/2$ or $3\pi/2$, the surface atoms migrate along the particle surface the farthest. In all, the force F drives the undulations of the particle surface accompanied by the fluctuations in the surface atoms.

For the supported particle, due to the limitation of its hemispherical truncation, θ ranges from 0 to α. For contact angles where $\alpha<\pi/2$, the maximum value of $\bar{v}$ is reached when θ equals α. For $\alpha>\pi/2$, the maximum always corresponds to $\theta=\pi/2$. As an approximation, we consider the maximum value of $\bar{v}$ to be the migration velocity V of the particle [57], and according to the Nernst-Einstein relation, the diffusion coefficient D of the particle can be written as

$$D(\alpha)=\frac{3C_pD_s\Omega^2}{2\pi r^4\alpha_1}C_\alpha, \tag{10}$$

where $C_\alpha=\sin\alpha,\alpha<\pi/2;C_\alpha=1,\alpha\geq\pi/2$.

The above derivation only addresses the effects of the particle shape or the degree of wetting. The migration of the particle by means of the flow of the surface atoms also involves the formation and cleavage of the chemical bonds of the perimeter atoms at the three-phase junction of the particle, support and vacuum. The interfacial adhesion energy E_{int} can be introduced to represent the energy barrier involved in the form of Arrhenius [61], then the diffusion coefficient can be represented as

$$D(\alpha)=\frac{3C_pD_s\Omega^2}{2\pi r^4\alpha_1}C_\alpha\exp\left(-\frac{E_{int}}{kT}\right), \tag{11}$$

where the diffusion coefficient D_s of the surface atoms over the particle surface is

$$\begin{aligned}D_s&=\frac{\lambda^2\nu_p}{4}\exp\left(\frac{\Delta S}{k}\right)\exp\left(-\frac{\Delta H}{kT}\right)\\&=S_{atom}\nu_p\exp\left(\frac{E_d^m}{kT}\right),\end{aligned} \tag{12}$$

where ν_p is the attempt frequency for particle surface atom hops, ΔS is the standard entropy change in the migration process and is assumed to be zero, ΔH is the standard enthalpy change and is equal to the diffusion barrier E_d^m, and λ is the hop length and is represented by $2\sqrt{S_{atom}}$. $S_{atom}=\pi r_{atom}^2$ and is the surface area occupied by a single atom. r_{atom} is the radius of a single atom. The particle surface atom density is

$$C_p=S_{atom}^{-1}\exp\left(-\frac{E_{sub}-E_{ad}^m}{kT}+\frac{2\Omega E_{sur}}{kTr}\right), \tag{13}$$

where E_{sub} is the sublimation heat of the bulk metal, E_{ad}^m is the adsorption energy of the metal atoms on the particle surface, and E_{sur} is the surface energy of the particle, which can be approximated by the bulk metal surface energy.

The diffusion of the particle on the support is a thermal activation process. The diffusion model proposed contains contributions from four physical aspects. The first aspect is the formation energy of a surface atom relative to its bulk phase counterpart ($E_{sub}-E_{ad}^m$). The second aspect is the diffusion barrier for a surface atom on the particle surface (E_d^m). The third aspect is the change in the activation energy due to the particle size, more precisely, the chemical potential of the atoms in the particle ($2\Omega E_{sur}/r$). The last aspect is that the migration of the perimeter atoms relative to the support requires the corresponding activation energy barrier to be surpassed. This barrier is related to the formation and cleavage of the chemical bonds between the particle and the support.

Mathematically, the support-related factors determining the diffusion rate of the particle mainly include three aspects: the first aspect is the radius of curvature r of the particle, the second aspect is the geometry factors (C_α and α_1) from the shape of the particle, and the third aspect is the interfacial adhesion energy (E_{int}) between the particle and the support. The contact angle α of a given particle mainly depends on the interfacial energy E_{int} based on the Young-Dupré relation $E_{int}=S_{atom}E_{sur}(1+\cos\alpha)$. For a supported hemispherical particle with a fixed volume $V_p=4\pi r^3\alpha_1/3$, the radius of curvature r depends on the contact angle α. In the ideal case, for a given particle, both α and r depend on E_{int}. Obviously, the interfacial energy E_{int} ultimately determines the migration rate of the particle.

If K_α is used to represent all the support-related effects during the particle diffusion, we obtain:

$$\begin{aligned}D(\alpha)&=\frac{3\nu_pC_\alpha\Omega^2}{2\pi r^4\alpha_1}\exp\left(-\frac{E_{tot}+E_{int}}{kT}+\frac{2\Omega E_{sur}}{kTr}\right)\\&=D_0C_\alpha/\alpha_1\exp\left(-\frac{S_{atom}E_{sur}(1+\cos\alpha)}{kT}\right)\\&=K_\alpha D_0,\end{aligned} \tag{14}$$

where D_0 is the previous diffusion coefficient without the support effects reported in ref. [62]. $E_{tot}=E_{sub}-E_{ad}^m+E_d^m$ describes the energy needed for the formation and migration

of metal atoms on the particle surface. K_α mainly depends on the contact angle α of the particle, namely, the E_{sur}.

3 Smoluchowski kinetic model

A mean field model that overcomes the statistical errors associated with the random collision method in a probabilistic way was adopted to simulate the particle migration and coalescence (PMC) kinetics [67,68]. In this approach, the particles are assumed to be distributed randomly on the support surface, and the probability of interparticle collision is proportional to the particle number density and mobility. The time-dependent particle number density of volume v, $f(v, t)$, is assumed to obey the following rate equation:

$$\frac{\partial f(v,t)}{\partial t} = \int_0^v D(v')f(v',t)f(v-v',t)\mathrm{d}v' - \int_0^{\infty}[D(v)+D(v')]f(v,t)f(v',t)\mathrm{d}v', \quad (15)$$

where $D(v)$ is the diffusion coefficient of a particle with volume v. The right-hand side of this equation consists of a term for gain and a term for loss. The term for gain represents the increments in the particle number density with volume v due to the coalescence of the particles with a volume v' and $v-v'$. This term is the sum of the probabilities of all the collision and coalescence events occurring between any two particles with a total volume v. The term for loss represents the reduction in the particle number density originating from the coalescence of the particles with a volume v with any other particles, including themselves. The net increment is equal to the gain minus the loss.

The kinetic simulation algorithm used to evolve the particle migration and coalescence kinetics was encoded via the method described in the ref. [62]. N particles are generated following a Gaussian size distribution with an average size $\langle d\rangle = 2\langle r\rangle$ and a standard deviation sd. Each generated particle is counted and grouped into n_b equally spaced bins based on the volume v ($4\pi r^3\alpha_1/3$) of the particle. The bins are sorted in monotonically increasing order and cover the range of all the particle volumes. The population corresponding to each bin (v_i) is indicated as $F_i = f(v_i)$. The diffusion coefficient $D_i = D(v_i)$ is given using eq. (14). The time evolution matrix can be given by

$$T_{ij} = F_i(D_jF_j). \quad (16)$$

T_{ij} is the collision rate of the particles with a volume v_j moving toward the particles with a volume v_i. This matrix multiplication provides all the information needed to determine the evolution of the particle size distribution (PSD) within a given time step. The change in the population of the particles with a volume v_i after dt is obtained by

$$\mathrm{d}f(v_i) = \sum_{k=i-j} T_{jk}\mathrm{d}t - \sum_j (T_{ij}+T_{ji})\mathrm{d}t, \quad (17)$$

where the first and second terms on the right-hand side represent the first and second integrals in eq. (15), respectively.

In addition to the migration and collision of particles [71–75], the subsequent coalescence process [24,72,76–85] is also important. Kinetic theory dealing with these two processes has been proposed by Ruckenstein et al. [22,23] considering that the diffusion of particles on the support is crucial in suppressing the sintering process [69,70,72,86], the simplified Smoluchowski kinetic model under diffusion-control conditions is adopted here. For particles capable of migration by means of the flow of the surface atoms, assuming their collision and subsequent fusion is reasonable. When the metal-support interaction is very weak, the contact angle of the particle is close to 180°. Thus, even if the particle lacks liquidity, the particle easily diffuses by rolling on the support. During this diffusion process, even though the particles collide, coalescence does not occur [74,75,87]. In the simulation, the contact angle is assumed to be constant for any particle size, and the defects on the support surface are not considered. These approximations do not affect the general conclusions of the effects of the metal-support interaction on the sintering resistance.

In actual situations, the support surface is always curved due to the crevices, pores and any other concave portions formed during the synthesis process. For substrate concavities whose dimensions/volumes are far larger than those of the supported particles, the corresponding kinetic model reduces to the case of a flat support very well. For substrate concavities whose dimensions are commensurate with those of the particles, the concavities in the substrate surface tend to make actual diffusion coefficients of the particles smaller than those that are given by the theoretical formula. As a reasonable assessment for these curved substrate materials in the nanoscale, the current work provides an upper limit for the particle migration. For microporous substrates, the particles are dispersed in the smallest pores. The coarsening of this class of particles is controlled by the sintering kinetics of the support phase, accompanied by the blunting or disappearance of certain substrate concavities, which is beyond the scope of this work.

4 Support-dependent diffusion coefficient

Five parameters determine the diffusion of a supported particle, i.e., the particle radius r, surface energy E_{sur}, total activation energy E_{tot}, contact angle α and temperature T. Figure 2(a) shows that the diffusion coefficient D changes with α and r for the three different versions. The black da-

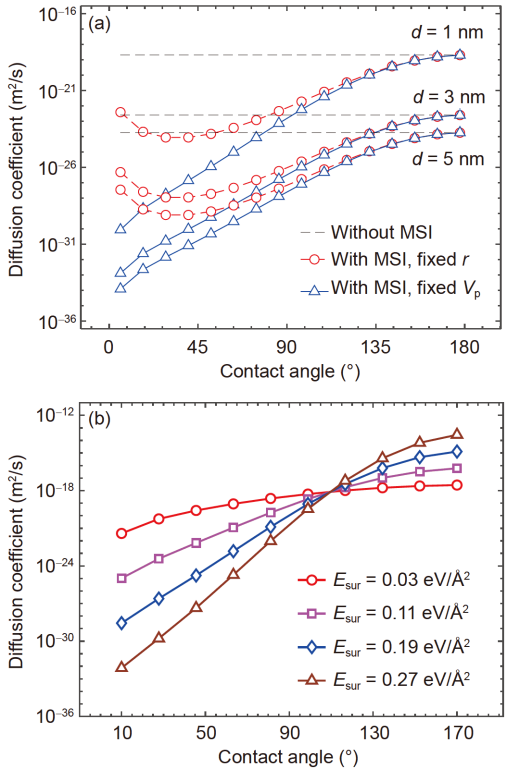

Figure 2 (Color online) Variation of the diffusion coefficients D of the three versions with the contact angle α under different particle diameters d (a) and surface energies E_{sur} (b). In (a), the model without MSI (D_0 in eq. (14)) is represented by black dashed lines. The red dashed lines with circles represent the new model with a fixed radius of curvature r (half of the diameter d) when α changes, namely, the particle volume V_p changes also. The blue solid lines with triangles correspond to a fixed V_p but a changing r. In each group of data, from top to bottom, the diameters of curvature are d = [1, 3, 5] nm, for α = 180°. d = 1 nm for α = 180° (for (b)), E_{tot} = 2.7 eV, Ω = 11.243 Å^3, E_{sur} = 0.15 eV/Å^2 (for (a)), T = 1330 K, $\nu_p = 6\times10^{13}$ s^{-1}.

shed lines represent the results from the previous model (D_0 in eq. (14)) without the metal-support interaction (MSI) effects. The red lines represent the results based on eq. (14) under fixed r; the blue lines are the results under conditions of a fixed particle volume V_p, where r changes implicitly with α. The black dashed lines of Figure 2(a) show that D_0 (in eq. (14)) decreases and that the rate of decrease gradually slows with increasing r. This behavior reflects the combined effects of the quartic reciprocal dependence of D_0 and the reciprocal dependence of the chemical potential of the atoms in the particle on the particle size r. However, D_0 does not change with α regardless of r. In the model without MSI (D_0), the concept of the contact angle does not exist, namely, MSI has no influence on the diffusion behavior. A supported particle shows the same diffusivity even when deposited on totally different supports, which is obviously not reasonable.

For the new diffusion model, as shown by the red dashed lines with circles and blue solid lines with triangles of Figure 2(a), D varies with decreasing α for each r. The enhanced E_{int} leads to a decreased α ($\arccos[E_{int}/(S_{atom}E_{sur})-1]$) and D is exponentially reduced as a result (eq. (14)). The fact that the geometry factor α_1 decreases rapidly with decreasing contact angle α, causes D to increase at a higher than exponential rate with decreasing α, for α smaller than approximately 90°. For a fixed r (the red lines in Figure 2(a)), the competition between the effects of the geometry and the interfacial interaction causes the diffusion coefficient D to first decrease and then increase with decreasing α. For larger α, the interfacial interaction dominates due to the small change in α_1, and D decreases with decreasing α. For smaller α, the sharply increasing contribution from the reciprocal of α_1 to D dramatically exceeds the contribution from the interfacial interaction, so a rapid reverse ascension occurs.

A decreasing α with a fixed r (the volume is not constant) is equivalent to removing the part of the particle below the contact surface with the support. However, the situation that we are concerned with is how the D of the whole particle changes with α, not portions of the particle (the blue lines with triangles in Figure 2(a)). The change in r should be naturally included in the effect of the support on a given particle. For a given particle (the blue lines with fixed V_p), the r ($\sqrt[3]{3V_p/4\pi\alpha_1}$) of the particle increases with decreasing α. The decrease of D due to increasing r ($1/r^4$ in eq. (14)) inverts the upward trend (shown by the red lines of Figure 2(a)) in D due to the geometry effects ($1/\alpha_1$) with decreasing α for smaller α. The geometry effect ($1/\alpha_1$) is conducive to the migration of the particle; an increased radius of curvature ($1/r^4$) and enhanced interfacial energy ($e^{-E_{sur}/kT}$) suppress the diffusion of the particle. In all, the suppression effects outweigh the promotion effects.

The three lines (black, red and blue) in Figure 2(a) for each d (1 nm, 3 nm and 5 nm for α = 180°) converge to the same value when α approaches 180°. The convergences show that the effect of the support becomes insignificant with weakening interaction until the new model (red and blue lines) totally degenerates back to the previous model (black lines). Figure 2(b) shows the dependence of the diffusion coefficient D on the contact angle α for different surface energies E_{sur}. A decreasing α results in a decreasing D, which reflects that strong interaction makes the diffusion of the particle difficult. The range of the variation of D increases with increasing E_{sur}, reflecting that the range of the interfacial interaction E_{int} is determined by E_{sur}. This range is the maximum value reached by modulating the support composition and structure. The results also show that a certain critical α_{cri} exists. For $\alpha < \alpha_{cri}$, D increases; for $\alpha = \alpha_{cri}$, D does not change, and for $\alpha > \alpha_{cri}$, D decreases with increasing E_{sur}. eq. (14) can be expressed as $\log(D) = k_{m1}(\alpha) + k_m E_{sur}$, where $k_{m1}(\alpha)$ is the parameter dependent on α, and $k_m = (2\Omega/r - S_{atom}(1+\cos\alpha))/kT$. These three situations correspond to $k_m > 0$, $k_m = 0$, $k_m < 0$, respectively. In the proposed model, E_{sur} not only determines the range of E_{int} but also the degree of re-

duction in the chemical potential $\Delta\mu(r) = 2\Omega E_{sur}/r$ of the atoms in the particle with increasing r. Increasing $\Delta\mu(r)$ with respect to higher E_{sur} results in an increase in the particle surface atom density C_p, thereby promoting particle diffusion. This effect is completely opposite to the inhibitory effect on D from increasing E_{int} due to increasing E_{sur}. Thus, when α is equal to α_{cri}, increasing E_{int} only has a negligible impact on D; when α is greater than α_{cri}, the promotion effect from increasing C_p prevails, and when α is less than α_{cri}, the inhibitory effect from increasing E_{int} dominates.

Figure 3(a) shows the dependence of the diffusion coefficient D on the contact angle α for different temperatures T. D increases with increasing T regardless of α. The degree of increase for smaller α is far greater than that for larger α. D increases from 10^{-55} m^2/s to 10^{-25} m^2/s for $\alpha = 6°$ and 10^{-20} m^2/s to 10^{-10} m^2/s for $\alpha = 178°$ with T from 400 K to 1600 K. The ranges of the variation in D with decreasing α significantly decrease with increasing T, from 35 to 15 orders of magnitude for an increase of 1200 K in T. Again, we consider the thermal activation of the diffusion behavior of the particle, namely, that the thermal kinetic energy needs to be high enough so that the particle can cross the diffusion barrier. The barrier contains contributions from the total activation energy E_{tot} of the surface atoms, the interfacial energy E_{int} and the chemical potential $\Delta\mu(r)$ of the atoms at the particle. The ability to cross the energy barrier is enhanced with increasing T, resulting in a higher D that overshadows the effects from the other factors.

Except for the promotion effect from $\Delta\mu(r)$ on D due to E_{sur}, the other two energy barriers, E_{tot} and E_{int}, both suppress the diffusivity. These two barriers have completely different sources. E_{tot} is determined by the properties of the material itself. E_{int} can be tuned by choosing a suitable support composition and surface structure. Figure 3(b) shows the dependence of D on α for different E_{tot}. These two factors have comparable influences on D. D decreases with increasing E_{int} or decreasing α regardless of E_{tot}. The higher the E_{tot}, the more difficult the formation and migration of the surface atoms, and the lower the D of the particle.

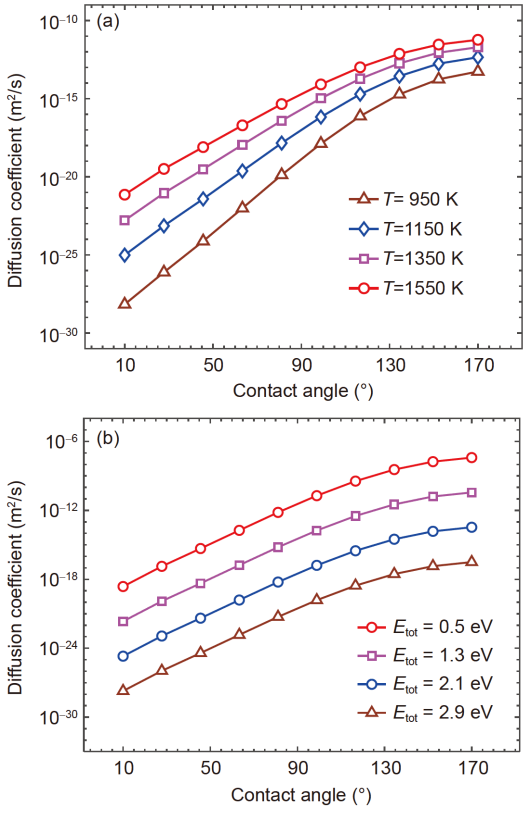

Figure 3 (Color online) Variation of the diffusion coefficient D with the contact angle α under different temperatures T (a) and total activation energies E_{tot} (b). d = 1 nm for α = 180°, E_{tot} = 2.7 eV (for (a)), E_{sur} = 0.15 eV/Å^2, Ω = 11.243 Å^3, T = 1330 K (for (b)), $\nu_p = 6\times10^{13}$ s^{-1}.

5 Support-dependent stability

Figure 4 shows that the PSD (Figure 4(a)) and normalized

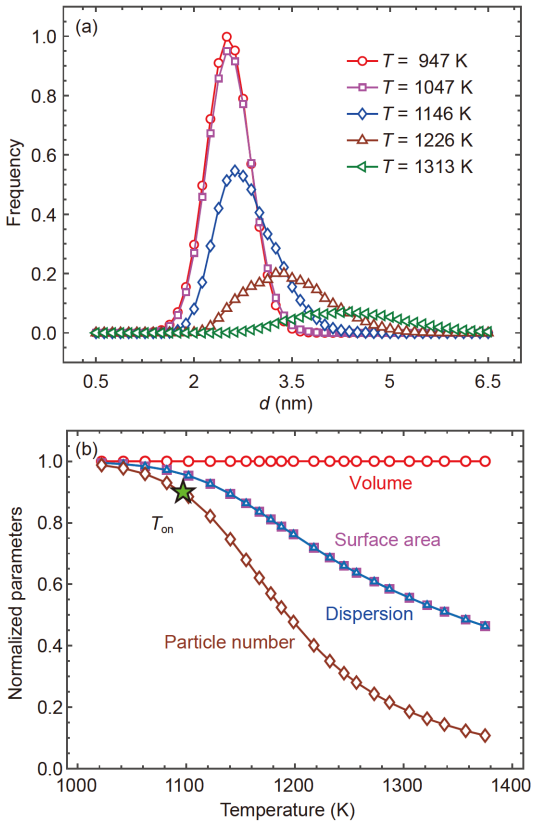

Figure 4 (Color online) Evolution of particle size distribution (PSD) (a) and normalized parameters (b) with increasing temperature T in a temperature ramping process for a supported particle ensemble undergoing the migration and coalescence process. In (a), selected PSDs at several different T points in the simulation are shown. In (b), the variations of the normalized volume, surface area, dispersion and particle number with increasing T are shown. Initial $\langle d \rangle$ = 2 nm, initial sd = 0.34 nm, α = 90°, E_{tot} = 2.15 eV, E_{sur} = 0.1 eV/Å^2, Ω = 11.243 Å^3, T_i = 800 K, R_T = 1 K/s, $\nu_p = 6\times10^{13}$ s^{-1}.

parameters (Figure 4(b)) evolve with increasing T during the temperature ramping process of a typical supported particle ensemble. In Figure 4(a), we plot the PSDs at several special temperatures. The results show that the peak widens with increasing T. The PSD has a long tail in the direction of the larger sizes and a steep slope in the direction of the smaller sizes, which is called a lognormal distribution, a typical feature of the particle migration and coalescence process. Figure 4(b) shows the evolution of certain statistical quantities with T. A constant total system volume indicates that the mass is strictly conserved. The total area, namely, the dispersion considering constant total volume, and the total particle number decreases quickly after reaching a specific T. The temperature at which the particle number has decreased to 90% of the initial value is defined as the onset temperature T_{on} [88].

Figure 5 shows the evolution of the statistical information during an isothermal kinetic. Figure 5(a) indicates the formation of a lognormal size distribution with a long tail toward the direction of the larger sizes from an initial Gaussian-like shape. This phenomenon is caused by the nature of PMC; the particle growth must involve the coalescence of particles into a whole. Figure 5(b) shows the variation of statistical quantities with time. As an indicator of mass conservation, the total volume is constant. As expected, the particle number, surface area and derived dispersion decrease due to the disappearance of the smaller particles. The rate of change of the dispersion or particle number slows in later stages. This result reflects that the rate of isothermal PMC slows and seems to enter a stable stage. The time when the total particle number has decreased to 50% of its initial value is defined as the half-life time $t_{1/2}$, which represents the sintering resistance of supported particles suffering from the PMC process.

We now use T_{on} and $t_{1/2}$ as indicators to study the support-dependence of the PMC kinetics of supported particles. Figure 6 shows that T_{on} changes with the contact angle α, which represents the interaction between the metal and support under different surface energies E_{sur} (Figure 6(a)) and total activation energies E_{tot} (Figure 6(b)). T_{on} decreases with increasing α, indicating that the thermal resistance deteriorates with weakening MSI. Extremely small E_{sur} (due to the adsorption of reactants [8]), for example, E_{sur} = 0.01 eV/ Å^2 (red line in Figure 6(a)), suppress the effects

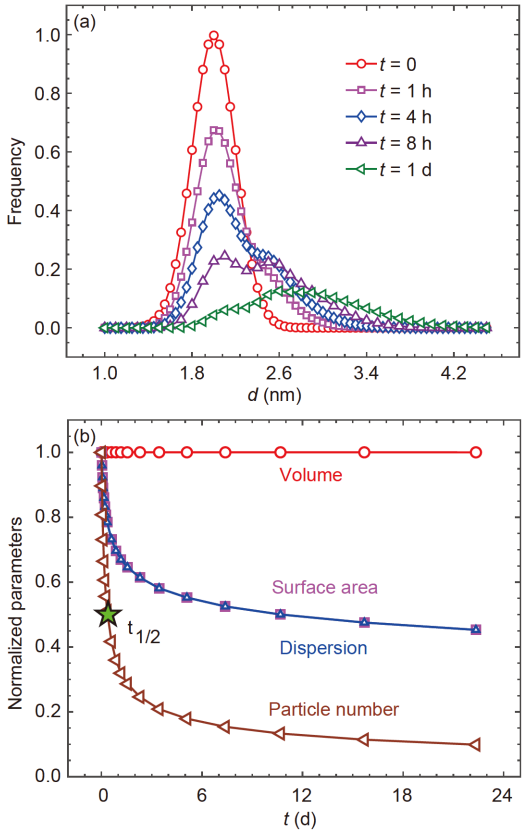

Figure 5 (Color online) Evolution of particle size distribution PSD (a) and normalized parameters (b) with time under a temperature aging process for a supported particle ensemble undergoing the PMC kinetics. Subfigure (a) shows selected PSDs at several times in this temperature aging process simulation. Subfigure (b) shows the normalized volume, surface area, dispersion and particle number with time. Initial $\langle d \rangle$ = 2 nm, initial sd = 0.2 nm, α = 90°, E_{tot} = 2.15 eV, E_{sur} = 0.1 eV/Å^2, Ω = 11.243 Å^3, T = 900 K, ν_p = 6×10^{13} s^{-1}.

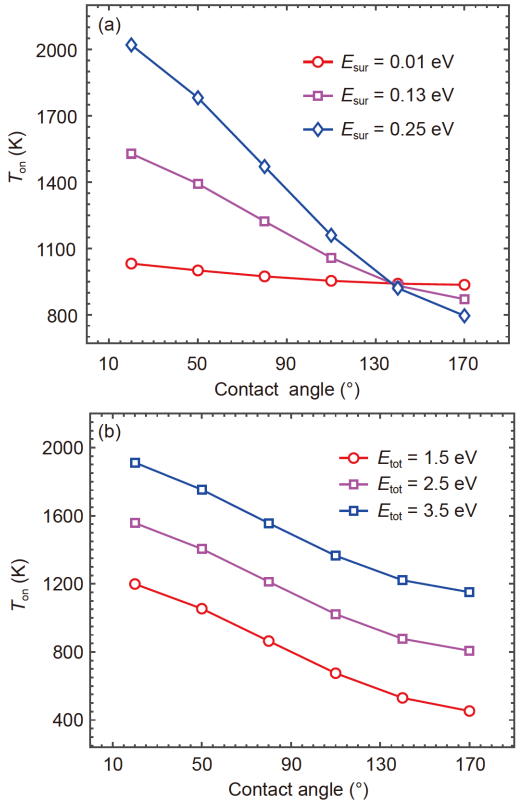

Figure 6 (Color online) Variation of the onset temperature T_{on} of a supported nanoparticle ensemble with contact angle (α) for different surface energies (E_{sur}) (a) and total activation energies (E_{tot}) (b). R_T = 1 K/s, ν_p = 6×10^{13} s^{-1}.

from the MSI.

An increase in E_{sur} leads to an increase in T_{on} for α smaller than approximately 130°. Otherwise, an increase in E_{sur} causes a decrease in T_{on}. The results show that an increase in E_{sur} suppresses the PMC process for strong MSI; however, an increase in E_{sur} promotes the PMC process for weak MSI. As discussed above (Figure 2(b)), the chemical potential $\Delta\mu(r)$ of the atoms in the particle increases and E_{int} decreases with increasing α. $k_m = (2\Omega/r - S_{atom}(1+\cos\alpha))/kT$ increases with increasing α. Since $k_m < 0$ for smaller α, an increase in E_{sur} leads to a decrease in D (Figure 2(b)), which enhances the suppression of the PMC process, namely, increasing T_{on} (Figure 6(a)). When $k_m > 0$ for larger α, an increase in E_{sur} promotes the PMC process, which is reflected by an increase in α resulting in a decrease in T_{on}. Figure 6(b) shows that increasing the total activation energy E_{tot} from 1.5 eV to 3.5 eV leads to an increase in T_{on} as high as 800 K for any α, which means that an increase in E_{tot} aids the suppression of the PMC process of supported particles.

Figure 7(a) shows the effect of the average diameter $\langle d \rangle$ on T_{on}. The results show that increasing size suppresses the PMC process. In Figure 7(b), the half-life time $t_{1/2}$ is used to measure the effects from α under different T. As a thermal activation process, T is expected to have a significant influence on the sintering resistance. Here, $t_{1/2}$ decreases from 10^{16} s to 10^{1} s for α = 45° and 10^{3} s to 10^{-5} s for α = 145° when T increases from 800 K to 1600 K. $t_{1/2}$ decreases with increasing T regardless of α. The range of the variation of $t_{1/2}$ with α significantly decreases with increasing T, from 15 to 8 orders of magnitude for an increase to 800 K for T. An increased temperature promotes the PMC process.

Figure 8 shows the particle volume distribution (PVD) at the same terminal conditions (T_s = 1300 K) in a temperature ramping process simulation from different initial contact angles α. With increasing α, the PVD shifts substantially to the right. The results show that increasing α, namely, weakening the metal-support interaction, promotes the PMC process from the perspective of particle volume distribution.

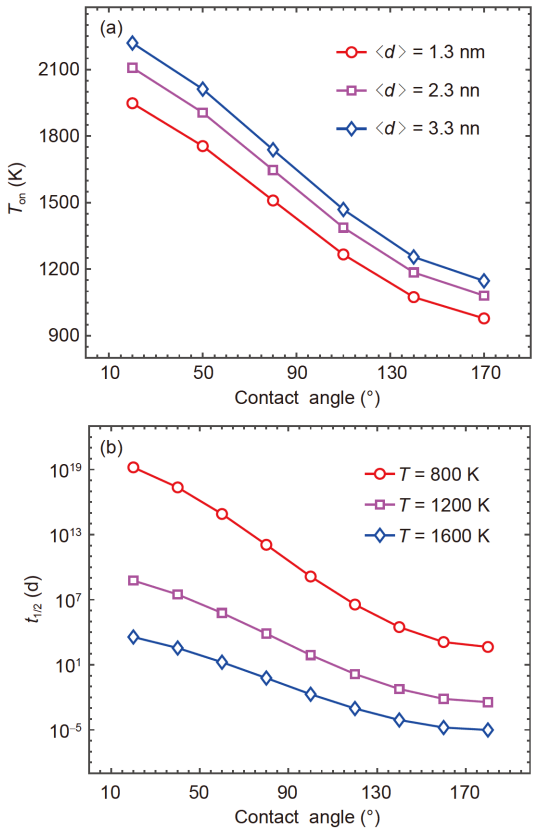

Figure 7 (Color online) (a) Variation of the onset temperature T_{on} of supported particles with contact angle (α) for different initial average diameters <*d*>; (b) half-life-time $t_{1/2}$ varies with α under different T. R_T = 1 K/s.

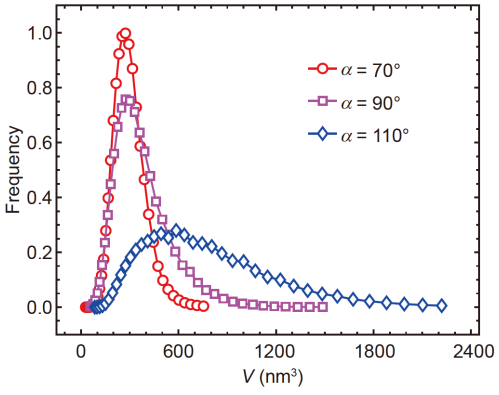

Figure 8 (Color online) Evolution of particle volume distribution (PVD) from the same initial PVD and terminal conditions (T_s = 1300 K) for selected α during a temperature ramping kinetic. $\langle d \rangle$ = 0.75 nm, sd = 0.15 nm for α = 180°, E_{sur} = 0.15 eV/Å^2, E_{tor} = 2.7 eV, Ω = 11.243 Å^3, T_i = 700 K, R_T = 1 K/s.

6 Conclusion

Developing theoretical descriptions and understanding the support-dependence of particle migration and coalescence (PMC) kinetics are challenging due to the lack of model theory for supported particle diffusion depending on metal-support interaction. Here, a new diffusion model that considers the support effects based on the surface premelting and Nernst-Einstein relation is proposed and expressed analytically. The PMC kinetics for supported particles are simulated based on the Smoluchowski ripening model. The results show that enhanced metal-support interaction can increase the radius of curvature and interfacial adhesion energy of supported particles, which inhibits their migration and coalescence, even though this interaction also decreases the geometry factor, promoting the PMC process. An increase in the particle surface energy can increase the interfacial interaction and surface atom density by improving the chemical potential of the atoms in a particle. The former is

conducive to the PMC process and the latter inhibits the process. A critical contact angle exists due to the competition between these two factors. An increased total activation energy and a decreased temperature are helpful in improving the migration resistance. This work provides a foundation for understanding the support effects on the migration and coalescence kinetics of supported particles.

This work was supported by the National Key R&D Program of China (Grant Nos. 2018YFA0208603, 2017YFB0602205), the Chinese Academy of Sciences (Grant No. QYZDJ-SSW-SLH054), and the National Natural Science Foundation of China (Grant No. 91645202).

1 Hansen T W, Delariva A T, Challa S R, et al. Sintering of catalytic nanoparticles: Particle migration or ostwald ripening? Acc Chem Res, 2013, 46: 1720–1730
2 Farmer J A, Campbell C T. Ceria maintains smaller metal catalyst particles by strong metal-support bonding. Science, 2010, 329: 933–936
3 Wanke S E, Flynn P C. The sintering of supported metal catalysts. Catal Rev, 1975, 12: 93–135
4 Astier M, Teichner S J, Vergnon P. Sintering and catalysis. In: Kuczynski G C, ed. Sintering and Catalysis. Materials Science Research. Boston: Springer, 1975. 10: 63–81
5 Wynblatt P, Gjostein N A. Supported metal crystallites. Prog Solid State Chem, 1975, 9: 21–58
6 Tao F F, Crozier P A. Atomic-scale observations of catalyst structures under reaction conditions and during catalysis. Chem Rev, 2016, 116: 3487–3539
7 DeLaRiva A T, Hansen T W, Challa S R, et al. In situ transmission electron microscopy of catalyst sintering. J Catal, 2013, 308: 291–305
8 Hu S, Li W X. Theoretical investigation of metal-support interactions on ripening kinetics of supported particles. ChemNanoMat, 2018, 4: 510–517
9 Liu J C, Wang Y G, Li J. Toward rational design of oxide-supported single-atom catalysts: Atomic dispersion of gold on ceria. J Am Chem Soc, 2017, 139: 6190–6199
10 Xu H, Cheng D, Cao D, et al. A universal principle for a rational design of single-atom electrocatalysts. Nat Catal, 2018, 1: 339–348
11 O'Connor N J, Jonayat A S M, Janik M J, et al. Interaction trends between single metal atoms and oxide supports identified with density functional theory and statistical learning. Nat Catal, 2018, 1: 531–539
12 Liu Z P, Jenkins S J, King D A. Role of nanostructured dual-oxide supports in enhanced catalytic activity: Theory of CO oxidation over $Au/IrO_2/TiO_2$. Phys Rev Lett, 2004, 93: 156102
13 Wahlström E, Lopez N, Schaub R, et al. Bonding of gold nanoclusters to oxygen vacancies on rutile TiO_2(110). Phys Rev Lett, 2003, 90: 026101
14 Sanz-Navarro C F, Åstrand P O, Chen D, et al. Molecular dynamics simulations of carbon-supported Ni clusters using the reax reactive force field. J Phys Chem C, 2008, 112: 12663–12668
15 Li C, Huang J, Li Z. A relation for nanodroplet diffusion on smooth surfaces. Sci Rep, 2016, 6: 26488
16 Liu X, Liu M H, Luo Y C, et al. Strong metal-support interactions between gold nanoparticles and ZnO nanorods in CO oxidation. J Am Chem Soc, 2012, 134: 10251–10258
17 Ta N, Liu J J, Chenna S, et al. Stabilized gold nanoparticles on ceria nanorods by strong interfacial anchoring. J Am Chem Soc, 2012, 134: 20585–20588
18 Lee J, Burt S P, Carrero C A, et al. Stabilizing cobalt catalysts for aqueous-phase reactions by strong metal-support interaction. J Catal, 2015, 330: 19–27
19 Qiao B, Liang J X, Wang A, et al. Ultrastable single-atom gold catalysts with strong covalent metal-support interaction (CMSI). Nano Res, 2015, 8: 2913–2924
20 Tang H, Wei J, Liu F, et al. Strong metal-support interactions between gold nanoparticles and nonoxides. J Am Chem Soc, 2016, 138: 56–59
21 Zhang S, Plessow P N, Willis J J, et al. Dynamical observation and detailed description of catalysts under strong metal-support interaction. Nano Lett, 2016, 16: 4528–4534
22 Ruckenstein E, Pulvermacher B. Kinetics of crystallite sintering during heat treatment of supported metal catalysts. AIChE J, 1973, 19: 356–364
23 Ruckenstein E. Growth kinetics and the size distributions of supported metal crystallites. J Catal, 1973, 29: 224–245
24 Wang J, Chen S, Cui K, et al. Approach and coalescence of gold nanoparticles driven by surface thermodynamic fluctuations and atomic interaction forces. ACS Nano, 2016, 10: 2893–2902
25 Luedtke W D, Landman U. Slip diffusion and Lévy flights of an adsorbed gold nanocluster. Phys Rev Lett, 1999, 82: 3835–3838
26 Lewis L J, Jensen P, Combe N, et al. Diffusion of gold nanoclusters on graphite. Phys Rev B, 2000, 61: 16084–16090
27 Yoon B, Luedtke W D, Gao J, et al. Diffusion of gold clusters on defective graphite surfaces. J Phys Chem B, 2003, 107: 5882–5891
28 Celestini F. Diffusion of a liquid nanoparticle on a disordered substrate. Phys Rev B, 2004, 70: 115402
29 Jensen P, Clément A, J. Lewis L. Diffusion of nanoclusters on non-ideal surfaces. Phys E-Low-dimensional Syst NanoStruct, 2004, 21: 71–76
30 Maruyama Y. Temperature dependence of Lévy-type stick-slip diffusion of a gold nanocluster on graphite. Phys Rev B, 2004, 69: 245408
31 Chen J, Chan K Y. Size-dependent mobility of platinum cluster on a graphite surface. Mol Simul, 2005, 31: 527–533
32 Alkis S, Krause J L, Fry J N, et al. Dynamics of Ag clusters on complex surfaces: Molecular dynamics simulations. Phys Rev B, 2009, 79: 121402
33 Ryu J H, Seo D H, Kim D H, et al. Molecular dynamics simulations of the diffusion and rotation of Pt nanoclusters supported on graphite. Phys Chem Chem Phys, 2009, 11: 503–507
34 Ma M, Tocci G, Michaelides A, et al. Fast diffusion of water nanodroplets on graphene. Nat Mater, 2016, 15: 66–71
35 Guerra R, Tartaglino U, Vanossi A, et al. Ballistic nanofriction. Nat Mater, 2010, 9: 634–637
36 Bogicevic A, Liu S, Jacobsen J, et al. Island migration caused by the motion of the atoms at the border: Size and temperature dependence of the diffusion coefficient. Phys Rev B, 1998, 57: R9459–R9462
37 Stoldt C R, Jenks C J, Thiel P A, et al. Smoluchowski ripening of Ag islands on Ag(100). J Chem Phys, 1999, 111: 5157–5166
38 Thiel P A, Shen M, Liu D J, et al. Coarsening of two-dimensional nanoclusters on metal surfaces. J Phys Chem C, 2009, 113: 5047–5067
39 Kang H C, Thiel P A, Evans J W. Cluster diffusivity: Structure, correlation, and scaling. J Chem Phys, 1990, 93: 9018–9025
40 Wen J M, Chang S L, Burnett J W, et al. Diffusion of large two-dimensional Ag clusters on Ag(100). Phys Rev Lett, 1994, 73: 2591–2594
41 Stankic S, Cortes-Huerto R, Crivat N, et al. Equilibrium shapes of supported silver clusters. Nanoscale, 2013, 5: 2448–2453
42 Mittendorfer F, Seriani N, Dubay O, et al. Morphology of mesoscopic Rh and Pd nanoparticles under oxidizing conditions. Phys Rev B, 2007, 76: 233413
43 Seriani N, Mittendorfer F. Platinum-group and noble metals under oxidizing conditions. J Phys-Condens Matter, 2008, 20: 184023
44 Shao X, Prada S, Giordano L, et al. Tailoring the shape of metal Ad-particles by doping the oxide support. Angew Chem Int Ed, 2011, 50: 11525–11527
45 Sterrer M, Risse T, Heyde M, et al. Crossover from three-dimensional to two-dimensional geometries of Au Nanostructures on thin MgO (001) films: A confirmation of theoretical predictions. Phys Rev Lett, 2007, 98: 206103
46 Jak M J J, Konstapel C, van Kreuningen A, et al. The influence of

substrate defects on the growth rate of palladium nanoparticles on a TiO_2(110) surface. Surf Sci, 2001, 474: 28–36
47 Wallace W T, Min B K, Goodman D W. The stabilization of supported gold clusters by surface defects. J Mol Catal A-Chem, 2005, 228: 3–10
48 Xu L, Henkelman G, Campbell C T, et al. Pd diffusion on MgO(100): The role of defects and small cluster mobility. Surf Sci, 2006, 600: 1351–1362
49 Plessow P N, Abild-Pedersen F. Sintering of Pt nanoparticles via volatile PtO_2: Simulation and comparison with experiments. ACS Catal, 2016, 6: 7098–7108
50 Gerber T, Knudsen J, Feibelman P J, et al. CO-induced smoluchowski ripening of Pt cluster arrays on the graphene/Ir(111) Moiré. ACS Nano, 2013, 7: 2020–2031
51 Matthey D, Wang J G, Wendt S, et al. Enhanced bonding of gold nanoparticles on oxidized TiO_2(110). Science, 2007, 315: 1692–1696
52 Lu P, Campbell C T, Xia Y. A sinter-resistant catalytic system fabricated by maneuvering the selectivity of SiO_2 deposition onto the TiO_2 surface versus the Pt nanoparticle surface. Nano Lett, 2013, 13: 4957–4962
53 Zhu H, Ma Z, Overbury S H, et al. Rational design of gold catalysts with enhanced thermal stability: Post modification of Au/TiO_2 by amorphous SiO_2 decoration. Catal Lett, 2007, 116: 128–135
54 Qian K, Huang W, Jiang Z, et al. Anchoring highly active gold nanoparticles on SiO_2 by CoO_x additive. J Catal, 2007, 248: 137–141
55 Zanella R, Rodríguez-González V, Arzola Y, et al. Au/Y-TiO_2 catalyst: High activity and long-term stability in CO oxidation. ACS Catal, 2012, 2: 1–11
56 Min B K, Wallace W T, Goodman D W. Synthesis of a sinter-resistant, mixed-oxide support for Au nanoclusters. J Phys Chem B, 2004, 108: 14609–14615
57 Gruber E E. Calculated size distributions for gas bubble migration and coalescence in solids. J Appl Phys, 1967, 38: 243–250
58 Willertz L E, Shewmon P G. Diffusion of helium gas bubbles in gold and copper foils. MT, 1970, 1: 2217–2223
59 Morgenstern K, Rosenfeld G, Poelsema B, et al. Brownian motion of vacancy islands on Ag(111). Phys Rev Lett, 1995, 74: 2058–2061
60 Khare S V, Bartelt N C, Einstein T L. Diffusion of monolayer adatom and vacancy clusters: Langevin analysis and Monte Carlo simulations of their Brownian motion. Phys Rev Lett, 1995, 75: 2148–2151
61 Jak M J J, Konstapel C, van Kreuningen A, et al. Scanning tunnelling microscopy study of the growth of small palladium particles on TiO_2 (110). Surf Sci, 2000, 457: 295–310
62 Behafarid F, Roldan Cuenya B. Coarsening phenomena of metal nanoparticles and the influence of the support pre-treatment: Pt/TiO_2 (110). Surf Sci, 2012, 606: 908–918
63 Parker S C, Campbell C T. Kinetic model for sintering of supported metal particles with improved size-dependent energetics and applications to Au on TiO_2(110). Phys Rev B, 2007, 75: 035430
64 Levitas V I, Samani K. Size and mechanics effects in surface-induced melting of nanoparticles. Nat Commun, 2011, 2: 284
65 Taylor A B, Siddiquee A M, Chon J W M. Below melting point photothermal reshaping of single gold nanorods driven by surface diffusion. ACS Nano, 2014, 8: 12071–12079
66 Kubo R. The fluctuation-dissipation theorem. Rep Prog Phys, 1966, 29: 255–284
67 Smoluchowski M V. Drei vorträge über diffusion, brownsche molekularbewegung und koagulation von kolloidteilchen. Physik Zeit, 1916, 17: 557–571
68 Kandel D. Selection of the scaling solution in a cluster coalescence model. Phys Rev Lett, 1997, 79: 4238–4241
69 Pluis B, Frenkel D, van der Veen J F. Surface-induced melting and freezing II. A semi-empirical Landau-type model. Surf Sci, 1990, 239: 282–300
70 Heyraud J C, Métois J J, Bermond J M. Surface melting and equilibrium shape; the case of Pb on graphite. J Cryst Growth, 1989, 98: 355–362
71 Wang S C, Ehrlich G. Diffusion of large surface clusters: Direct observations on Ir(111). Phys Rev Lett, 1997, 79: 4234–4237
72 José-Yacaman M, Gutierrez-Wing C, Miki M, et al. Surface diffusion and coalescence of mobile metal nanoparticles. J Phys Chem B, 2005, 109: 9703–9711
73 Kébaili N, Benrezzak S, Cahuzac P, et al. Diffusion of silver nanoparticles on carbonaceous materials. Cluster mobility as a probe for surface characterization. Eur Phys J D, 2009, 52: 115–118
74 Bardotti L, Jensen P, Hoareau A, et al. Experimental observation of fast diffusion of large antimony clusters on graphite surfaces. Phys Rev Lett, 1995, 74: 4694–4697
75 Bardotti L, Jensen P, Hoareau A, et al. Diffusion and aggregation of large antimony and gold clusters deposited on graphite. Surf Sci, 1996, 367: 276–292
76 Yang W C, Zeman M, Ade H, et al. Attractive migration and coalescence: A significant process in the coarsening of $TiSi_2$ islands on the Si(111) surface. Phys Rev Lett, 2003, 90: 136102
77 Arcidiacono S, Bieri N R, Poulikakos D, et al. On the coalescence of gold nanoparticles. Int J Multiphase Flow, 2004, 30: 979–994
78 Asoro M A, Kovar D, Shao-Horn Y, et al. Coalescence and sintering of Pt nanoparticles: *In situ* observation by aberration-corrected HAADF STEM. Nanotechnology, 2010, 21: 025701
79 Yuk J M, Jeong M, Kim S Y, et al. *In situ* atomic imaging of coalescence of Au nanoparticles on graphene: Rotation and grain boundary migration. Chem Commun, 2013, 49: 11479
80 Jiang Y, Wang Y, Zhang Y Y, et al. Direct observation of Pt nanocrystal coalescence induced by electron-excitation-enhanced van der Waals interactions. Nano Res, 2014, 7: 308–314
81 Li J, Wang Z, Chen C, et al. Atomic-scale observation of migration and coalescence of Au nanoclusters on YSZ surface by aberration-corrected STEM. Sci Rep, 2015, 4: 5521
82 Niu K Y, Liao H G, Zheng H. Visualization of the coalescence of bismuth nanoparticles. Microsc Microanal, 2014, 20: 416–424
83 Goudeli E, Pratsinis S E. Crystallinity dynamics of gold nanoparticles during sintering or coalescence. AIChE J, 2016, 62: 589–598
84 Han Y, Stoldt C R, Thiel P A, et al. *Ab initio* thermodynamics and kinetics for coalescence of two-dimensional nanoislands and nanopits on metal (100) surfaces. J Phys Chem C, 2016, 120: 21617–21630
85 Zheng H, Smith R K, Jun Y W, et al. Observation of single colloidal platinum nanocrystal growth trajectories. Science, 2009, 324: 1309–1312
86 Pluis B, van der Gon A W D, van der Veen J F, et al. Surface-induced melting and freezing I. Medium-energy ion scattering investigation of the melting of Pb{hkl} crystal faces. Surf Sci, 1990, 239: 265–281
87 Aydin C, Lu J, Browning N D, et al. A "smart" catalyst: Sinter-resistant supported iridium clusters visualized with electron microscopy. Angew Chem Int Ed, 2012, 51: 5929–5934
88 Hu S, Li W X. Influence of particle size distribution on lifetime and thermal stability of Ostwald ripening of supported particles. ChemCatChem, 2018, 10: 2900–2907